Joint Sampling Rate and Quantization Rate-Distortion Analysis in 5G Compressive Video Sensing

Jin-xiu Zhu[1,2], Christian Esposito[3], Aimin Jiang[1,2], Ning Cao[4], Pankoo Kim[5]

[1] College of Internet of Things Engineering, Hohai University, China
[2] Jiangsu Provincial Collaborative Innovation Center of World Water Valley and Water Ecological Civilization, China
[3] Department of Computer Science, University of Salerno, Italy
[4] College of Computer and Information, Hohai University, China
[5] Department of Computer Engineering, Chosun University, South Korea
19941489@hhu.edu.cn, 20111837@hhu.edu.cn, esposito@unisa.it, 20020009@hhu.edu.cn, pkkim@chosun.ac.kr

Abstract

Compressed video sensing (CVS) is one of the 5G application of compressed sensing (CS) to video coding. Block-based residual reconstruction is used in CVS to explore temporal redundancy in videos. However, most current studies on CVS focus on random measurements without quantization, and thus they are not suitable for practical applications. In this study, an efficient rate-control scheme combining measurement rate and quantization for residual reconstruction in CVS is proposed. The quantization effects on CS measurements and recovery for video signals are first analyzed. Based on this, a mathematical relationship between quantitative distortion (QD), sampling rate (SR), and the quantization parameter (QP) is derived. Moreover, a novel distortion model that exhibits the relationship between QD, SR, and QP is presented, if statistical independency between the QD and the CS reconstruction distortion is assumed. Then, using this model, a rate–distortion (RD) optimized rate allocation algorithm is proposed, whereby it is possible to derive the values of SR and QP that maximize visual quality according to the available channel bandwidth.

Keywords: Residual reconstraction compressed video sensing, Rate-distortion model, Quantitative parameters, Sampling rate

1 Introduction

A key demanding aspect of 5G solutions is to provide capabilities that must extend far beyond what available in the previous generations of mobile communications. Such aspects involve very high data rates, very low latency, ultra-high reliability, energy efficiency and extreme device densities. In particular, 5G will be the cornerstone for the connectivity in the upcoming applications made possible by the progressive implementations of the Internet of Things and Smart Cities concepts, paving the way to the so-called Networked Society [1-3]. For these reasons, security and privacy represent two demanding aspects that 5G solutions must provide in order to become a platform for the future above-mentioned networked infrastructures for public communication and people empowerment. Specifically, 5G will have to face novel requirements in terms of security and privacy imposed by the upcoming applications, and will have to face a novel threat landscape and an increased concern for privacy. The security level provided by the current 4G systems is high and standardized with built-in security functions since the second generation (GSM) systems. However, the novel upcoming applications will surely require additional capacity, so in 5G the offered security capacities cannot be the carbon copy of the ones in 4G, but must be their evolution, as in any other aspect mentioned before. It is important, therefore, to point out these novel requirements, determining if the existing 4G security capacity are sufficient, and/or determining the novel solutions so as to have a step forward to meet the demands in the security and privacy of wireless communications [4-7].

In traditional video acquisition, Shannon's sampling theorem is applied to uniformly sample a large amount of data at or above the Nyquist sampling rate. To facilitate efficient storage and/or transmission of videos, compression algorithms are applied to remove redundancy and convert a large amount of raw data into a relatively small bit stream. Compressed sensing (CS) [8-9] is a framework for signal sensing and compression that provides a new scheme for collecting data at a rate that could be below the Nyquist rate. It has attracted increasing attention over the past few years. Based on CS, compressed video sensing (CVS) [10-12] is suitable for low-complexity applications, owing to the great reduction of the sampling rate (SR), power consumption, and computational complexity.

*Corresponding Author: Pankoo Kim; E-mail: pkkim@chosun.ac.kr
DOI: 10.3966/160792642020012101018

As in the case of rate control [13] for conventional video coding schemes, rate allocation also plays an important role in the CVS framework. Without rate control, underflow and overflow of the client buffer may occur owing to the mismatching between the encoding bit rate and the available channel bandwidth. A large number of rate allocation algorithms for CVS have recently been developed. A novel method was proposed in [14]; it adaptively allocates the SR according to the ratio of the image block variance to the frame variance. However, these techniques only explore the spatial redundancy within frames by independently considering each frame in the sequence and fail to address temporal redundancy in videos. To explore the temporal correlation and achieve higher sampling efficiency, in [15] a block-based adaptive framework is proposed for CVS that classifies blocks into different types depending on their inter-frame correlation and adjusts the sampling and reconstruction strategy accordingly.

However, all of the above rate control algorithms focus on SR allocation for real-valued measurements without considering the effect of quantization distortion and coding rate. In practice, however, the measurements are mapped to finite bits. Thus, in addition to SR, QP (quantization parameter) is another important factor for CVS in that it can regulate the encoded bit stream. QP can be effectively used to control the bit rate, so that the coding efficiency may be maximized with the constraints imposed by the channel rate, the encoder buffer size, and the decoder buffer size. To the best of the authors' knowledge, only the method introduced in [16] is designed for an adaptive CVS framework with a simple mode-based rate allocation, where SR and quantization bit-depth are jointly optimized. Although it can improve the coding efficiency of fixed quantization and accurately reach the target bit rate, it is still based on fitting the experimental data to rough models for computing the parameters.

To overcome these limitations, it is highly desirable to develop a more efficient distortion model that exhibits the relationship between distortion, SR, and QP for rate control in the CVS encoder. In this study, uniform scalar quantization is introduced into residual reconstruction CVS framework (RRCVS), and a more efficient method is proposed for realizing rate control. The proposed technique first uses the statistical and theoretical analysis of quantitative distortion (D_q) caused only by uniform scalar quantization to the measurements. Then, the CS reconstruction distortion (D_q^{CS}) caused by the quantization error is considered. Based on this, a useful statistic about the relations between D_q^{CS} , SR, and QP is obtained and a new SR–QP– D_q^{CS} model is derived. Moreover, the CS distortion (D_{cs}) caused only by compressed sampling without considering quantization is discussed, and a SR–QP– D_{cs} model is constructed. Furthermore, a novel SR–QP–D model is presented that exhibits the relationship between distortion, SR, and QP based on the assumption of statistical independency between D_q^{CS} and D_{cs} . Using this model, an RD-optimized rate allocation algorithm is proposed, whereby the values of SR and QP are derived so as to maximize the visual quality according to the available channel bandwidth. Then, an adaptive RRCVS framework with RD optimized rate allocation is presented that primarily comprises four modules: residual variance feedback, block type determination, bit allocation, and residual reconstruction. Experimental results demonstrate that the proposed scheme significantly improves the RD performance compared to the conventional methods.

The remainder of this paper is organized as follows. In Section 2, the basic compressed sensing theory is reviewed and the proposed adaptive RRCVS framework is introduced. In Section 3, a novel SR–QP–D model that exhibits the relationship between distortion, SR, and QP is proposed for block-based RRCVS. Based on the proposed model, a joint sampling rate and quantization optimization method is presented in Section 4. In Section 5, some experimental results are provided to evaluate the proposed algorithm. Finally, Section 6 concludes the paper.

2 Adaptive RRCVS Framework

2.1 Compressed Sensing

Compressive sensing is a framework for reconstruction of signals that have sparse representations. A signal x is called S-sparse if it has at most S nonzero entries. That is, a signal $x \in \Re^N$ can be sparsely represented with respect to some basis $\Psi_{N\times N} = [\psi_1, \psi_2, \cdots \psi_N]$, where ψ_i represents the i-th basis column vector, if $x = \Psi\alpha$ and the transform coefficient $\alpha \in \Re^N$ has only $S << N$ nonzero elements. Given a signal $x \in \Re^N$ that is S-sparse with respect to Ψ , compressed sensing explores the sparsity of the signal and takes only $M << N$ measurements during the sampling process. According to CS theory, the signal can be acquired through the linear random projections

$$y = \Phi x = \Phi\Psi\alpha \quad \textbf{(1)}$$

where Φ is an $M \times N$ measurement matrix, and $y \in \Re^M$ is the resulting measurement vector. As for compressive image, scrambled block Hadamard ensembles (SBHEs) [17-18], are mostly considered appropriate choices for Φ . As $M << N$, compressed sampling is a dimension reduction process, that is, it

facilitates the reduction of the size of the collected data. Here, the sampling rate of the signal is defined as

$$SR = M / N \tag{2}$$

According to CS, the reconstruction can be formulated as an l_1 -minimization problem [9] by solving

$$\hat{\alpha} = \arg\min \|\alpha\|_1 \qquad s.t.\, y = \Phi\Psi\alpha \tag{3}$$

where $\|\alpha\|_1$ is the l_1 norm of α. According to [9], when Φ is drawn randomly from a Gaussian or Bernoulli distribution and Ψ is an orthobasis, the solution $\hat{x} = \Psi\hat{a} \in \Re^N$ to (3) is unique with overwhelming probability. To solve this optimization problem, several techniques have been proposed, e.g., orthogonal matching pursuit (OMP) [19] and gradient projection for sparse reconstruction (GPSR) [20]. Furthermore, with high probability, we have the approximation

$$D_R = \|\hat{x} - x\|_2 \le C \ \|\alpha\|_p \left(\frac{M}{\log N}\right)^{0.5-1/p} \tag{4}$$

where $\|\alpha\|_p$ is the l_p -norm of the transform coefficient α, and C is a constant depending only on $P \in (0,2)$. Substituting (2) in (4) yields

$$D_R = \|\hat{x} - x\|_2 \le C \ \|\alpha\|_p \left(\frac{SR\ N}{\log N}\right)^{0.5-1/p} \tag{5}$$

2.2 Block-based Compressed Video Sensing

Videos involve a large amount of redundancy, which provides the basis for CS algorithms. However, CS faces several challenges including a computationally expensive reconstruction process and large memory requirements for storing the random sampling matrices. For video, these problems can be even further exacerbated owing to the increased dimension of the data. Fortunately, the sampling-operator memory issue was addressed for still images in [21] by using block-based sampling (BCS). Additionally, in [21], block-based CS with smooth projected Landweber (BCS-SPL) was proposed for fast reconstruction and smoothness with the goal of improving the quality of the reconstructed image by eliminating blocking artifacts. Experimental results in [21] demonstrated that BCS-SPL reconstruction usually offers at least the same quality of recovery as other state-of-the-art approaches with greatly increased execution speed. From the perspective of the incoherence principle in CS, block-based measurements appear to be less efficient than frame-based measurements. However, by sacrificing a part of the incoherence, BCS can preserve local information, thus facilitating the construction of more accurate side information (SI) by the decoder, based on the interframe sparsity model and sparsity-constraint block prediction for CVS. Recently, a distributed compressive video sensing (DCVS) framework has been proposed by Mun and Fowler [22], where the block-based measurement of a CS-frame is used to form a block-by-block MH motion-compensated prediction of the CS-frame. In [23], an alternative strategy for incorporating MH prediction into BCS-SPL video reconstruction was proposed.

In this study, an adaptive BCS-SPL residual reconstruction CVS framework with RD optimized rate allocation is proposed, where both SR and QP can be computed using a novel distortion model. Thereby, the optimal values of SR and QP can be adaptively assigned to each block using a feedback channel, thus resulting in improved RD performance.

2.3 Proposed RRCVS Framework with RD Optimized Rate Allocation

The proposed framework is illustrated in Figure 1. The frames of a video sequence are divided into two categories: key frames (also called K-frames) and non-key frames (also called CS-frames). Each frame is divided into several non-overlapping blocks of size $n \times n$. Each block in the K-frames is sampled and reconstructed using the regular compressed sensing technique, as shown at the bottom of Figure 1, whereas each block in the CS-frame is encoded with the assigned SR and QP. From the view point of the joint sparsity model in distributed compressed sensing (DCS) [24], SR is set higher in K-frames than in CS-frames, as the K-frames are usually reconstructed with better quality. The difference of the measurements (measurement residuals) between the block in a CS-frame and that at the same position in the previous K-frame is transmitted to the decoder, as video signals have large temporal redundancy and the inter-frame difference is significantly sparser than in the original frame.

Residual variance feedback. Based on the assumption that two successive frames in a video should be similar, the sparsity of each residual block is exploited to estimate the sparsity of the spatially co-located residual block that will be subsequently encoded. Alternatively, based on the fact that the complexity and the sparsity of an image are highly correlated, the variance of each block is proposed for rate–distortion analysis. Hence, the variance of the reconstructed residual block (V_R) at the decoder is computed and is fed back to the encoder.

Rate-distortion analysis. As shown in Figure 1, for the first CS-frame, the blocks are first sampled with the assigned SR and reconstructed using the regular compressed sensing technique. Then, the residual variance is computed and the block is classified. A novel rate–distortion model that exhibits the relationship between QD, SR, and QP is presented with the assuming statistical independency between the

quantitative distortion (QD) and the CS reconstruction distortion.

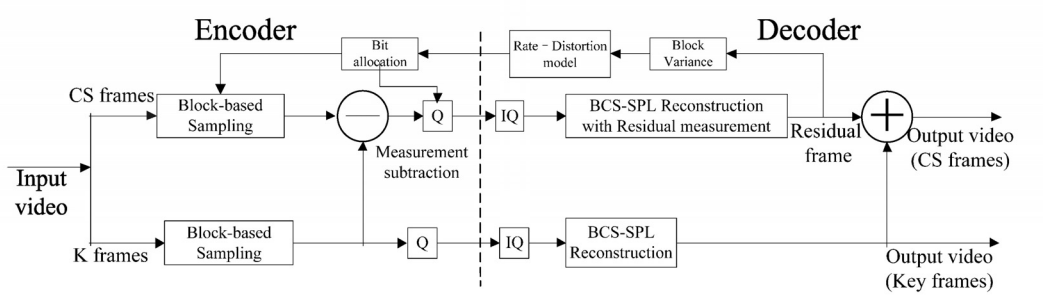

Figure 1. Proposed RRCVS framework with rate–distortion analysis

Bit allocation. SR and QP will be computed by the proposed distortion model according to the given target bit-rate. Thus, the RD optimized sampling rate can be estimated for video acquisition.

Residual reconstruction. After the video is adaptively acquired at R_T , the residual measurements are de-quantified and used for BCS-SPL [21] reconstruction to generate the residual frame in a block-by-block fashion. Then, the CS-frame is reconstructed by adding the residual reconstructed frame to the previously reconstructed K-frame.

3 Modeling Distortion for RRCVS

In this section, the effect measurement quantization on reconstruction distortion for video signals is first analyzed. Based on this, a mathematical relationship between quantitative distortion (QD), SR, and QP is derived. Then, the sampling rate effects on reconstruction distortion.

Moreover, the joint distortion caused by compressed sampling and quantization is analyzed. To this end, a novel distortion model that exhibits the relationship between distortion, SR, and QP is proposed.

3.1 Modeling Quantitative Distortion for Block-based Video Compressed Sensing

Herein, the distortion caused only by uniform scalar quantization to the measurements without considering the CS reconstruction is discussed. The measurement testing system for quantization distortion is shown in Figure 2. The frames of a video sequence are divided into two categories: K-frames and CS-frames. Both K-frames and CS-frames adopt consistent block-based random measurement, and we have

$$y = y_{CS} - y_K = \Phi x_{CS} - \Phi x_K = \Phi x \tag{6}$$

where y_{CS} and y_K are the measurement vectors of x_{CS} and x_K , respectively. The difference between the current block x_{CS} in a CS-frame and its co-located block in x_K in a K-frame is denoted by x . The residual information x is not available at the decoder in real systems. In this study, the same SBHE matrix [17] is used as the measurement matrix Φ for all blocks.

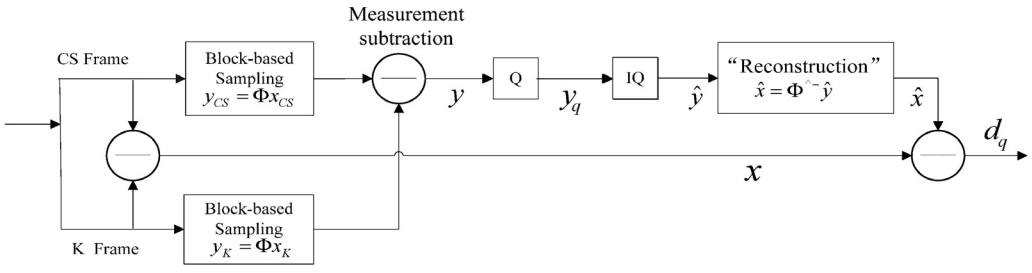

Figure 2. Testing system for measurement quantization distortion

Let Q denote the quantization function. Thus, quantifying the measurements y at the encoder can be denoted by

$$y_q = Q(\Phi x) \tag{7}$$

Let now IQ denote the inverse quantization function. Then $\hat{y} = IQ(y_q)$ is achieved at the decoder. Thus, the error d_{yq} caused by measurement quantization is

$$d_{yq} = \hat{y} - y \tag{8}$$

where, $d_{yq} = \left\{ d_{yq}^1, d_{yq}^2 \cdots d_{yq}^{N_B} \right\}$, d_{yq}^j is the error vector for the i-th block of the original frame, and N_B is the total number of blocks in a frame. For uniform quantization with quantization step size $\Delta = 2QP$, d_{yq} follows a uniform distribution with mean 0 and variance $\Delta^2/12$. Reconstructing $\hat{y}$ without considering

the error caused by the CS reconstruction algorithm, we have

$$\hat{x} = \Phi^{\wedge -} \hat{y} \tag{9}$$

where $\Phi^{\wedge -}$ is the pseudo-inverse matrix of $R_M = M / N$. Therefore, the distortion caused by quantization d_q is

$$d_q = x - \hat{x} = \Phi^{\wedge -} y - \Phi^{\wedge -} \hat{y} = \Phi^{\wedge -} (y - \hat{y}) = \Phi^{\wedge -} d_{yq} \tag{10}$$

Here, d_q^j is the distortion vector for the j-th block and can be represented as

$$d_q^j = \Phi^{\wedge -} d_{yq}^j = \left\{ \left\langle \phi_1, d_{yq}^j \right\rangle, \left\langle \phi_2, d_{yq}^j \right\rangle, \cdots \left\langle \phi_N, d_{yq}^j \right\rangle \right\}' \tag{11}$$

where $\{\phi_1, \phi_2, \cdots \phi_N\}$ is the row vector of $\Phi^{\wedge -}$ and N is the number of pixels in each block. The k-th element of d_q^j , $d_q^j(k)$ can be represented as

$$d_q^j(k) = \left\langle \phi_k, d_{yq}^j \right\rangle = \sum_{m=1}^{M} \phi_k(m) \cdot d_{yq}^j(m) \tag{12}$$

where M is the total number of measurements in each block. As the measurement matrix Φ must satisfy the restricted isometry property (RIP) [8], an i.i.d. Gaussian matrix is often used. In this situation, the distribution of CS coefficients would be expected to be Gaussian. By the central limit theorem, the (weighted) sum of identically distributed random variables can be well approximated by a Gaussian random variable. Therefore, by (11) and (12), d_q follows a Gaussian distribution with mean 0 and variance $\frac{\Delta^2}{12} \cdot M \cdot C$. Consequently,

$$p(d_q) = \frac{1}{\sqrt{2\pi}\sigma} e^{\left\{ -\frac{(d_q)^2}{2\sigma^2} \right\}} \tag{13}$$

Substituting $M = SR \cdot N$ into $\sigma^2 = \frac{\Delta^2}{12} \cdot M \cdot C$ yields

$$\sigma^2 = \frac{N}{12} \cdot C \cdot SR \cdot \Delta^2 \tag{14}$$

Where c is a constant, and the video SR is defined by $SR = M / N$. The experiment indicates that d_q shown in (13) approximately follows a Gaussian distribution with mean 0 and variance $\frac{N}{12} \cdot C \cdot SR \cdot \Delta^2$, which is not associated with sequences. Thus, the average quantization distortion D_q is

$$\begin{aligned} D_q &= \sqrt{\int_{-\infty}^{\infty} (d_q)^2 p(d_q) d(d_q)} \\ &= \sqrt{\int_{-\infty}^{\infty} (d_q)^2 \frac{1}{\sqrt{2\pi}\sigma} e^{\left\{ -\frac{d_q^2}{2\sigma^2} \right\}} d(d_q)} = \sigma \end{aligned} \tag{15}$$

Substituting (14) into (15) yields

$$\begin{aligned} D_q &= \sqrt{N/12 \cdot C \cdot SR \cdot \Delta^2} \\ &= \sqrt{N/12 \cdot C \cdot SR \cdot 4 \cdot QP^2} = k_1 \cdot \sqrt{SR} \cdot QP \end{aligned} \tag{16}$$

The above formula models the relationship between D_q , the quantization step size Δ (or QP) and SR. The testing results for D_q in Figure 1 under different SR for four sequences with N = 256 are shown in Figure 3, where QP is 4 and 8. It can be seen that the reconstruction error caused by quantization is associated with QP and MR, and is sequence-independent.

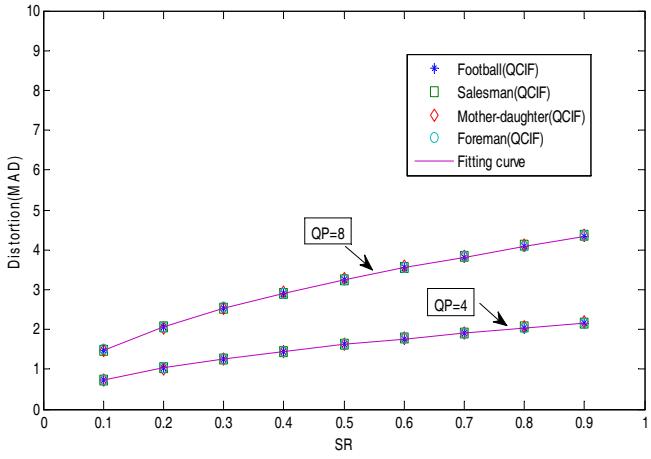

Figure 3. $D_q - SR$ curve with fixed

The CS reconstruction distortion D_q^{CS} caused by measurement quantization error for is now discussed. The D_q^{CS} testing system is shown in Figure 4. From the above discussion, the relationship between D_q^{CS}, QP, and SR is modeled by (16), that is

$$D_q^{CS} = k_2 \cdot \sqrt{SR} \cdot QP \tag{17}$$

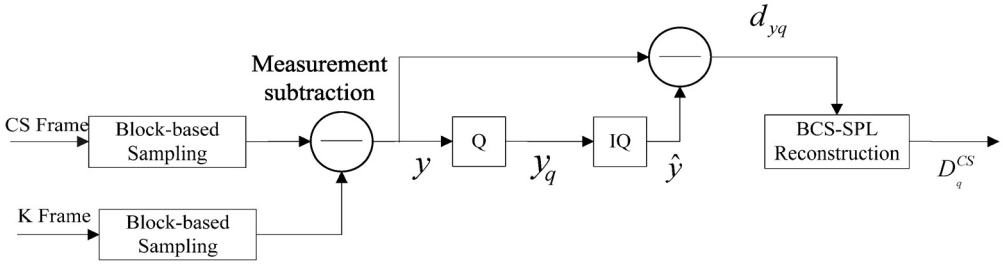

Figure 4. Testing system for CS distortion

The testing results for D_q^{CS} under different QP for four sequences with N = 256 are shown in Figure 5. QP was fixed, and the average distortion D_q^{CS} was calculated when SR increases from 0.1 to 0.8 for the "Foreman" and "Mother–daughter" QCIF and CIF sequences. It can be seen that D_q^{CS} is associated with the sequence format and is sequence-independent.

The testing results for D_q^{CS} under different QP for four sequences with N = 256 are shown in Figure 5. QP was fixed, and the average distortion D_q^{CS} was calculated when SR increases from 0.1 to 0.8 for the "Foreman" and "Mother–daughter" QCIF and CIF sequences. It can be seen that D_q^{CS} is associated with the sequence format and is sequence-independent.

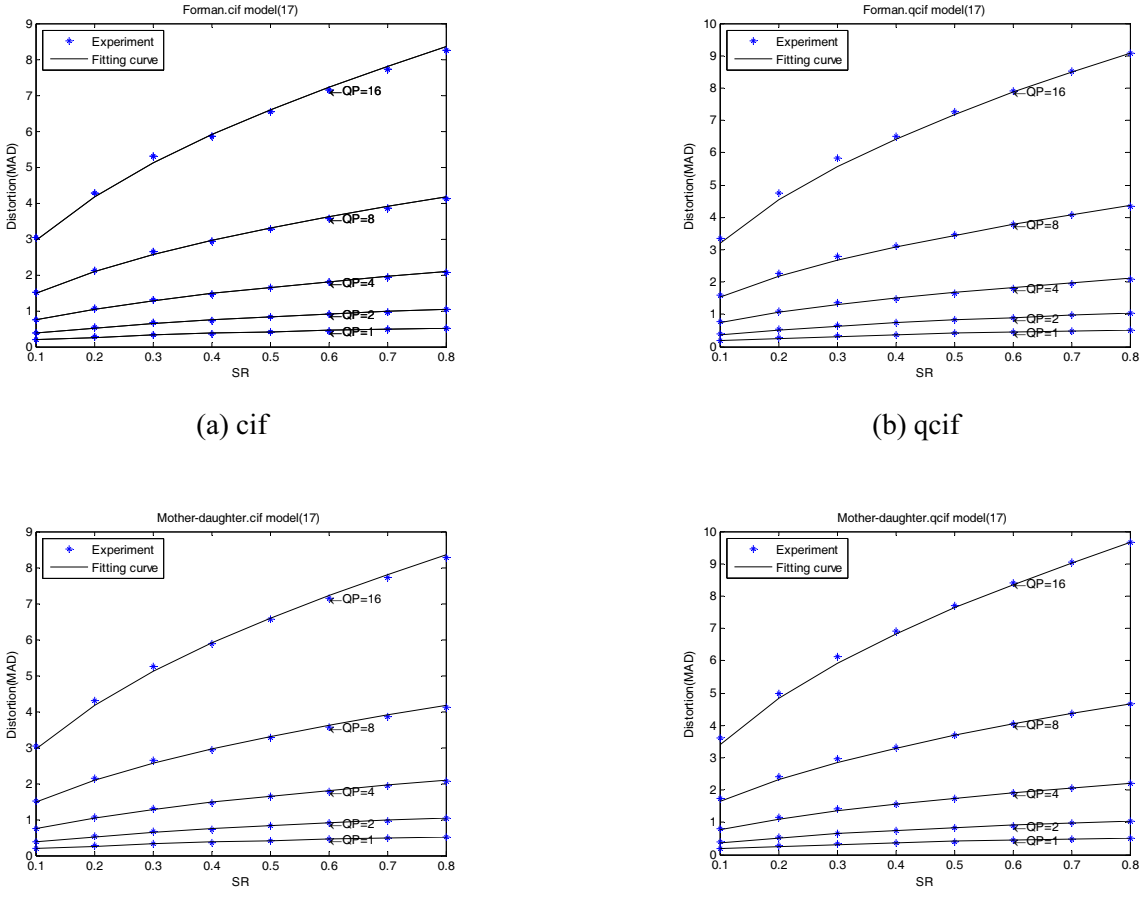

(a) cif

(b) qcif

(c) cif

(d) qcif

Figure 5. $D_q - SR$ curve with fixed QP

To evaluate the accuracy of the fitting, the Pearson correlation coefficient (PCC) was calculated, as well as the root mean square error (RMSE) between the measured and predicted D_q^{CS} .Table 1 presents the parameters of model (17) obtained by least squares fitting with fixed quantization parameters (QP =1, 2, 4, 8, 16, 32, 64, 128, and 256) when B increased from 0.1 to 0.8 with step 0.1. It can be seen that the model (17) has high PCC and low RMSE on average.

Table 1. Parameters and performance of model (17)

QP	Foreman.qcif			Foreman.cif			Mother-daughter.qcif			Mother-daughter.cif		
	C1	PCC	RMSE	C1	PCC	RMSE	C1	PCC	RMSE	C1	PCC	RMSE
1	0.5837	0.9993	0.0004	0.5832	0.9992	0.0004	0.5828	0.9992	0.0004	0.5834	0.9993	0.0004
2	0.5842	0.9993	0.0008	0.5838	0.9992	0.0008	0.5881	0.9992	0.0008	0.5834	0.9993	0.0008
4	0.5909	0.9986	0.0019	0.5831	0.9992	0.0017	0.6184	0.9988	0.0018	0.5833	0.9992	0.0017
8	0.6089	0.9972	0.0049	0.5832	0.9992	0.0034	0.6516	0.9984	0.0039	0.5841	0.9992	0.0035
16	0.6352	0.9967	0.0109	0.5832	0.9992	0.0067	0.6746	0.9986	0.0077	0.5831	0.9993	0.0068
32	0.6633	0.9976	0.0200	0.5828	0.9992	0.0134	0.6887	0.999	0.0136	0.5848	0.9994	0.0122
64	0.6859	0.9986	0.0341	0.5823	0.9992	0.027	0.6968	0.9993	0.0245	0.5902	0.9977	0.0344
128	0.7011	0.999	0.0726	0.5870	0.9991	0.0457	0.7011	0.9994	0.049	0.6127	0.9937	0.1089
256	0.7179	0.9974	0.2832	0.6125	0.9991	0.1116	0.7096	0.9979	0.224	0.6666	0.9957	0.3169

3.2 Modeling CS Distortion for Block-based Video Compressed Sensing

Herein, the CS distortion (D_{cs}) caused only by compressed sampling without considering the quantization is discussed. The testing system for CS distortion is shown in Figure 6. For each block in a CS-frame, the difference in the measurements (residual measurements) between a block in a CS-frame and that at the same position in the previous K-frame is transmitted to the decoder. Residual measurements are used for BCS-SPL [21] reconstruction to generate the residual frame. Then, the CS-frame is reconstructed by adding the residual frame to the reconstructed K-frame, as shown at the top of Figure 6. The testing results of D_{cs} under different SR for the "Football", "Foreman", "News" and "Mother–daughter" sequences with N = 256 are shown in Figure 6, where the two sets of CIF and QCIF sequences are used.

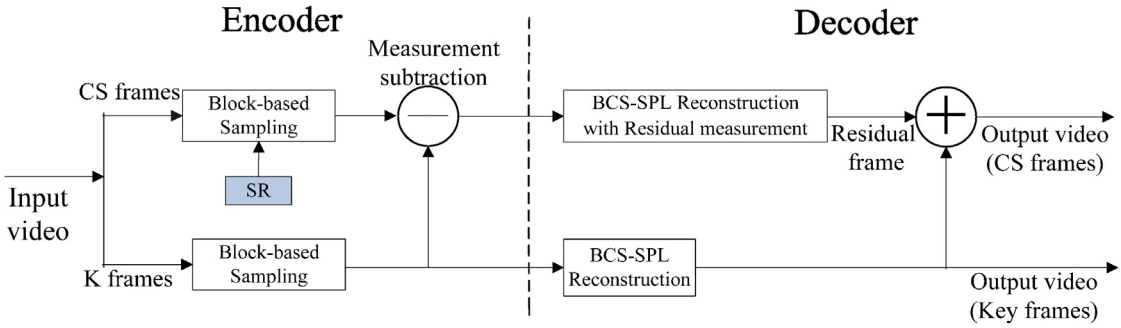

Figure 6. CS distortion testing system

As shown in Figure 7, the average distortion D_{cs} is calculated as SR increases from 0.1 to 0.8 for the above four sequences. It can be seen that for the "Football" sequence with fast or complex motion, the distortion is rapidly reduced. However, for sequences with slow motion and relatively simple scene composition, such as the "Mother–daughter sequence", SR is slowly reduced. The average residual variance, denoted by V_R , for the blocks of the "Football", "Foreman", "News", and "Mother–daughter" CIF sequences is 20.9529, 5.3328, 1.2745, and 1.3162, respectively. The average V_R for the blocks of the "Football", "Foreman", "News", and "Mother–daughter" QCIF sequences is 28.1829, 3.1301, 1.1498, and 0.8229, respectively. Moreover, it can also be observed that D_{cs} increases as V_R increases. Thus, D_{cs} is related to SR and V_R .

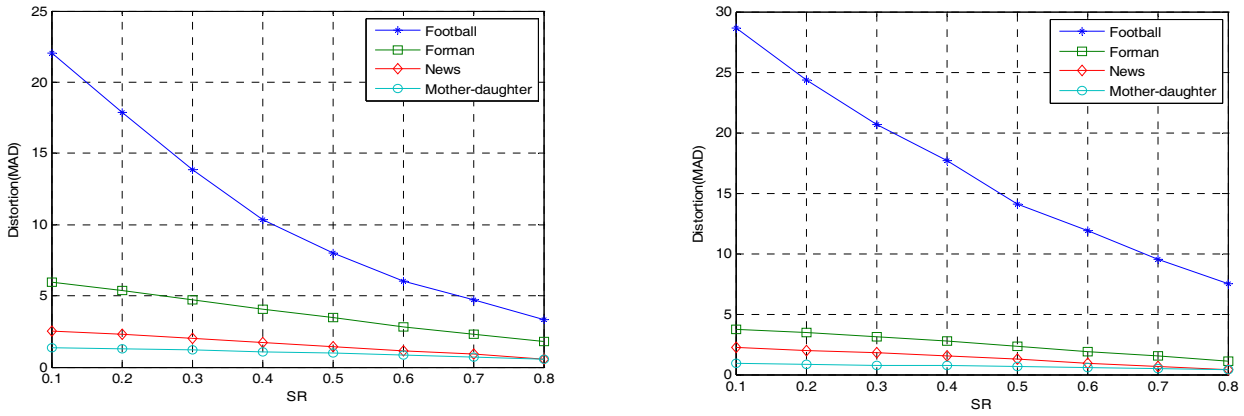

(a) cif (b) qcif

Figure 7. $D_{CS} - SR$ curve without quantization. (a) cif (b) qcif

D_{cs} is assumed to depend on SR and the sparsity of the signal. Based on the fact that the complexity and sparsity of an image are highly correlated, V_R is used to approximately express sparsity. For the "Foreman", "News", and "Mother–daughter" sequences, it can be seen from Figure 7 that D_{cs} increases with SR approximately linearly because these sequences have simple motion, and residual blocks can be sparsely represented. More sparse blocks require fewer measurements. Thus, SR = 0.1 is sufficiently large to obtain high reconstruction quality. Hence, it is assumed that

$$D_{cs} = V_R \cdot (k_1.SR + k_2) \tag{18}$$

The parameters are estimated by least squares fitting for the data obtained. To quantify the accuracy of the fitting, PCC is calculated, as well as the RMSE between the measured and predicted D_{cs}. Table 2 summarizes the model parameters obtained by least squares fitting, and shows that the model provides a PCC of 0.972 and a RMSE of 0.7984 on average. However, for the "Football" The experimental data for model (19) for both QCIF and CIF video sequences are shown in Figure 8, where both the measured and the predicted results are plotted. It can be observed that the model provides a reasonable approximation of the relationship.sequence with complex motion, which requires more measurements, D_{cs} decreases rapidly as SR increases. That is, D_{cs} changes with SR nonlinearly. Equation (5) suggests that the relationship between D_{cs} and the two factors can be modeled as

$$\begin{aligned} D_{cs} &= w_1 \cdot V_R \cdot (k_1.SR + k_2) + V_R \cdot \frac{k_3}{SR^{k_4}} + V_R \cdot k_5 \\ &= V_R \cdot (k'_1.SR + k'_2) + V_R \cdot \frac{k_3}{SR^{k_4}} \end{aligned} \tag{19}$$

Table 2. Parameters and performance of model (18)

	CIF				QCIF				Average
	Football	News	Mother daughter	Forman	Football	News	Mother -daughter	Forman	
k_1	−1.2743	−2.2877	−0.2961	−1.2114	−1.1146	−2.3032	−1.1555	−1.3385	
k_2	1.0534	2.4218	0.3368	1.2477	1.0572	2.3797	1.4157	1.3396	
PCC	0.9570	0.9501	0.9745	0.9881	0.9694	0.9770	0.9784	0.9815	0.9720
RMSE	2.8457	0.0652	0.0193	0.0880	3.2291	0.0535	0.0151	0.0714	0.7984

Table 3 summarizes the model parameters obtained by least squares fitting, and shows that the model has high PCC and small RMSE on average. From Tables 2 and 3, it can be observed that the RMSE (2.8457) for model (19) for "Football" is significantly smaller than the RMSE (1.1475) for model (18). However, it can also be observed that the RMSE remains stable for the other three sequences. Thus, model (18) is better suited for sequences with simple motion, whereas model (19) for sequences with complex motion.

Table 3. Parameters and performance of model (19)

	CIF				QCIF				Average
	Football	News	Mother -daughter	Forman	Football	News	Mother -daughter	Forman	
k'_1	−0.4729	−2.5853	−1.2852	−0.9704	−0.5951	−2.6227	−1.4592	−1.1625	
k'_2	0.0012	1.1800	0.5021	0.3017	0.0764	1.1642	0.6856	0.3788	
k_3	0.4517	1.4882	0.927	0.7558	0.5808	1.4799	0.9811	0.8210	
k_4	0.3986	−0.0807	−0.0415	0.1028	0.2438	−0.0876	−0.1305	0.0716	
PCC	0.9935	0.9996	0.9987	0.9901	0.9944	0.9976	0.9987	0.9956	0.9960
RMSE	1.1475	0.0636	0.0192	0.0760	2.1149	0.0524	0.0148	0.0688	0.4447

3.3 Modeling Distortion for Block-based Video Compressed Sensing

Herein, the joint distortion (D) caused by compressed sampling and quantization is discussed. The testing system for CS distortion is shown in Figure 9, which is similar to Figure 6, except for considering quantizing in the measurements.

It is assumed that the distortion caused by quantization and MR are independent. According to (17) and (19), the RD model based on CS can be expressed as

$$\begin{aligned} D &= w_2 \cdot D_q^{CS} + w_3 \cdot D_{cs} \\ &= w_2 \cdot k_2 \cdot \sqrt{SR} \cdot QP + w_3 \cdot \left[V_R \cdot (k'_1 .SR + k'_2) + V_R \cdot \frac{k_5}{SR^{k_6}} \right] \\ &= C_1 \cdot \sqrt{SR} \cdot QP + V_R \cdot (C_2 .SR + C_3) + V_R \cdot \frac{C_4}{SR^{C_5}} \end{aligned} \tag{20}$$

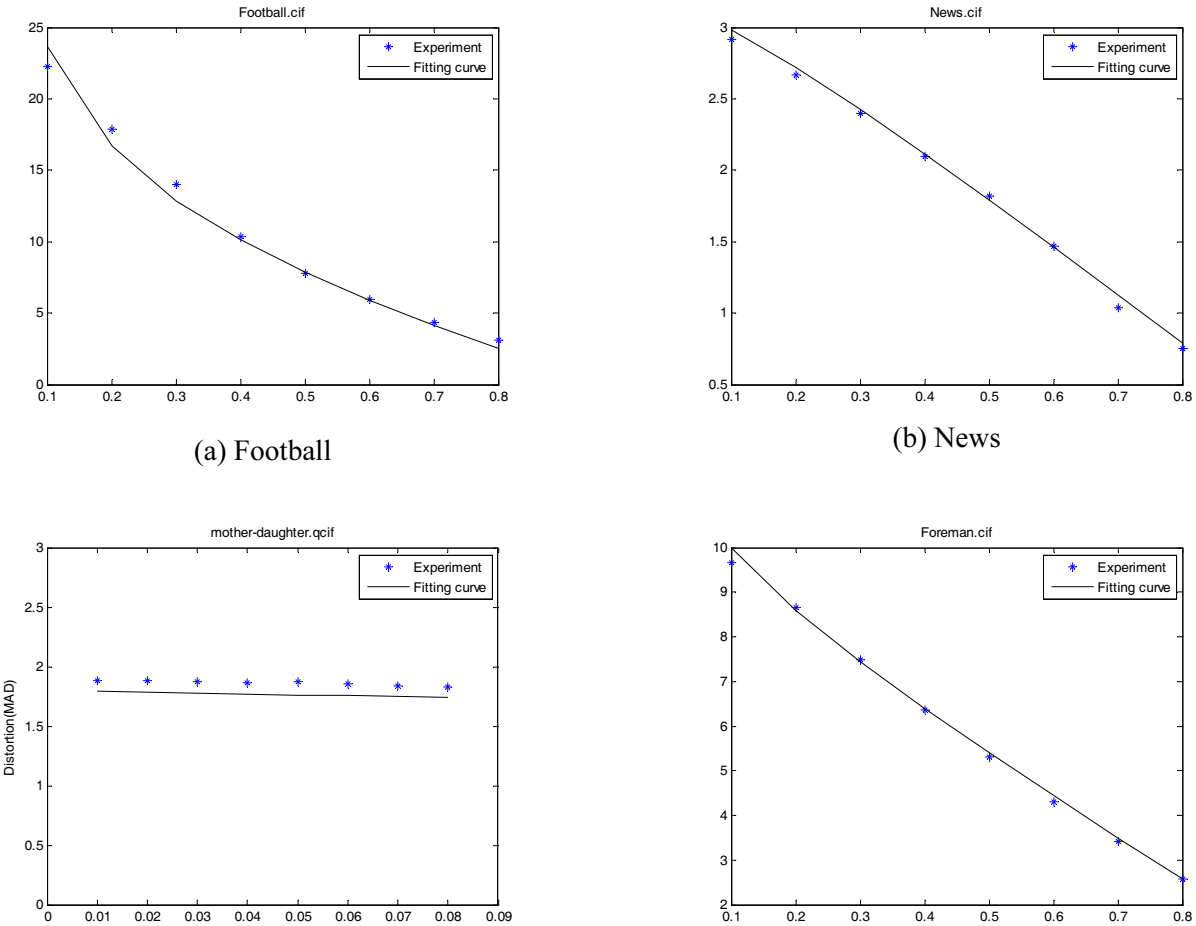

(a) Football (b) News

(c) Mother–daughter (d) Foreman

Figure 8. $D_{CS} - SR$ curve for CIF format sequence without quantization

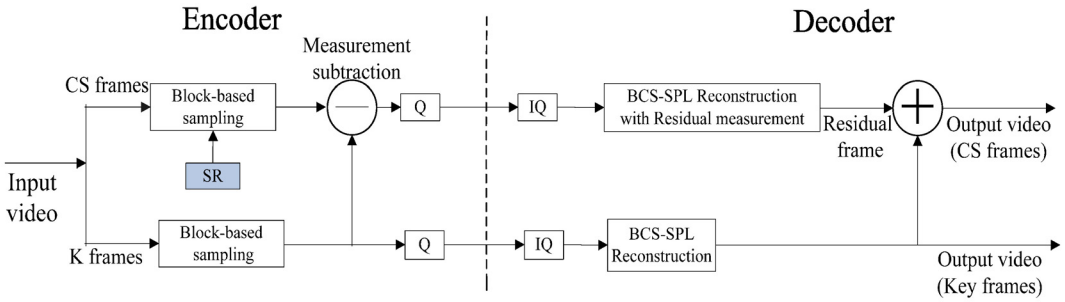

Figure 9. CS distortion testing system

The data is fitted to model (20), and the parameters are computed by least squares fitting. After the experiments, it can be observed that parameter C_4 approaches zero as QP increases, particularly for the sequences with simple motion. The most obvious reason is that as QP increases, the distortion caused by compressed sampling can be neglected and D is mainly caused by the effect of quantization. Hence, using $C_4 \approx 0$, model (20) can be simplified as

$$D = C_1 \cdot \sqrt{SR} \cdot QP + V_R \cdot (C_2 .SR + C_3) \qquad \textbf{(21)}$$

Furthermore, the system shown in Figure 9 was run numerous times with varying QP and SR, and the reconstruction distortion for QCIF and CIF sequences with different temporal and spatial characteristics was observed. The data was fitted to the models, and the parameters were computed by least squares fitting. To evaluate the performance of the two models, their RMSE were experimentally compared. To quantify the accuracy of the fitting, their RMSE were also compared with those in Liu et al. [16]. Table 4 shows the results with fixed quantization parameters (QP = 1, 2, 4, 8, 16, 32, 64, 128, and 256) as B increases from 0.1 to 0.8 with step 0.1. It can be seen that both model (20) and model (21) have better fitting performance than that in Liu et al. [16].

Table 4. Performance of model (20), model (21), and the model in [16]

	Foreman.cif			Mother-daughter.cif			News.cif			Football.cif		
RMSE / QP	Model (20)	Model (21)	Liu et al. [16]	Model (20)	Model (21)	Liu et al. [16]	Model (20)	Model (21)	Liu et al. [16]	Model (20)	Model (21)	Liu et al. [16]
1	0.0172	0.0188	0.0779	0.0091	0.0091	0.0283	0.0138	0.0138	0.0297	0.0684	0.1072	0.2405
2	0.0166	0.0189	0.0744	0.0097	0.0098	0.0269	0.0127	0.0132	0.0258	0.0678	0.1080	0.2375
4	0.0155	0.0194	0.0675	0.0100	0.0105	0.0242	0.0129	0.0130	0.0204	0.0662	0.1097	0.2306
8	0.0142	0.0212	0.0591	0.0087	0.0095	0.0197	0.0100	0.0111	0.015	0.0626	0.1103	0.2195
16	0.0142	0.0236	0.049	0.0063	0.0070	0.0241	0.0069	0.0075	0.0144	0.0568	0.1100	0.2042
32	0.0143	0.0227	0.0548	0.0061	0.0065	0.0653	0.0119	0.0146	0.0298	0.0487	0.1062	0.1771
64	0.0141	0.0181	0.1419	0.0120	0.0121	0.159	0.0251	0.0288	0.0638	0.0405	0.0897	0.1643
128	0.0231	0.0237	0.3522	0.0246	0.0246	0.3715	0.0499	0.0478	0.1675	0.0691	0.0798	0.3175
256	0.1156	0.1170	0.9461	0.1013	0.1024	0.9727	0.2029	0.1141	0.2349	0.2215	0.2244	0.8975

Moreover, model (20) has the best fitting performance and the smallest RMSE for sequences with complex motion, e.g., the "Football" sequence. Furthermore, as QP increases, the improvement of the performance for model (20) is negligible and even fails when QP = 128 and 256 for the "News" sequence. The most obvious reason is that as QP increases, the distortion is primarily due to the effect of quantization. Thus, model (20) is suitable for sequences with complex motion when QP < 5; otherwise, model (21) is better for sequences with slow motion. Here, "Mother–daughter" and "News" were tested in the simulations using model (21). The results are shown in Figure 10, where QP was set to 1, 2, 4, 8, and 16. It can be observed that model (21) provides a reasonable approximation of the relationship for sequences with slow motion.

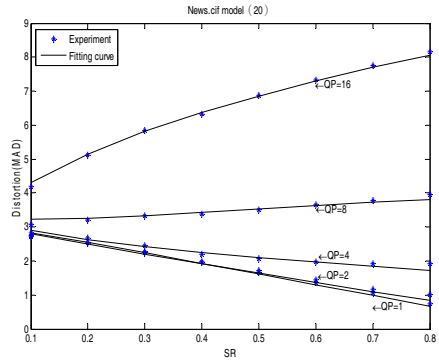

(a) Model (20) for News.cif

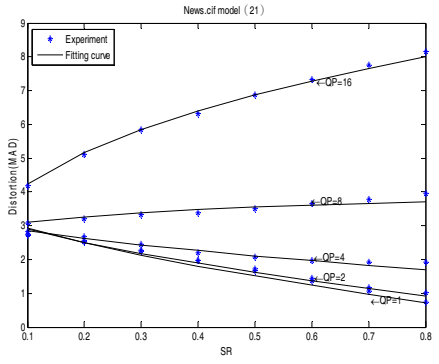

(b) Model (21) for News.cif

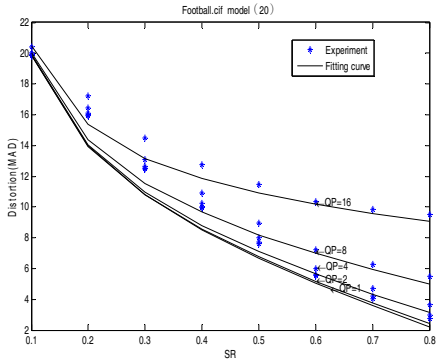

(c) Model (20) for Football.cif

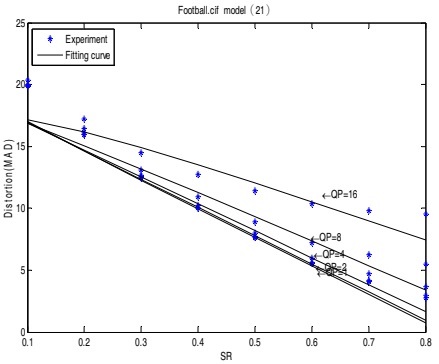

(d) Model (21) for Football.cif

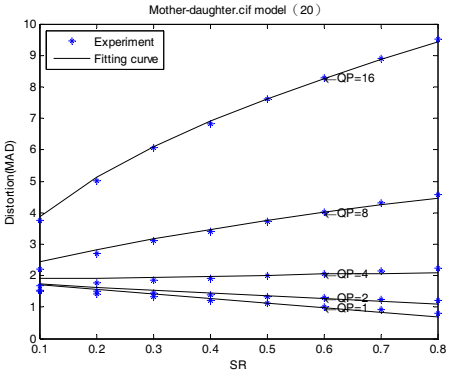

(e) Model (20) for Mother-daughter.cif

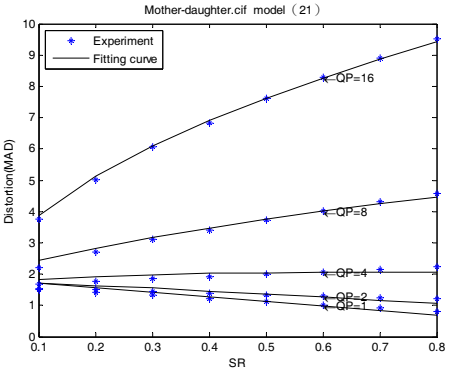

(f) Model (21) for Mother-daughter.cif

Figure 10. $D-SR$ curve for three sequences with fixed QP

To quantify the accuracy of the fitting, the PCC between the measured and predicted values was computed. The performance comparison for sequences including "Foreman", "Mother–daughter", and "News" between model (21) and Liu et al. [16] under the same conditions is shown in Tables 5-7. It can be seen that for CIF sequences, the average RMSE of model (21) is smaller by 0.7128 compared with that obtained by Liu et al. [16] (0.6665 for "Foreman", 0.8224 for "Mother–daughter", and 0.6495 for "News") as SR increases from 0.1 to 0.8. For QCIF sequences, the average RMSE of model (21) is smaller by 0.7606 compared with that obtained by Liu et al. [16] (0.7604 for "Foreman", 0.8253 for "Mother–daughter", and 0.6941 for "News"). It can also be seen that for QCIF sequences, the average PCC of model (21) is larger by approximately 0.0335 compared with that in Liu et al. [16] (0.0309 for "Foreman", 0.0351 for "Mother–daughter", and 0.0346 for "News"). For QCIF sequences, the average PCC of model (21) is larger by approximately 0.0343 compared with that in Liu et al. [16] (0.0327 for "Foreman", 0.0354 for "Mother–daughter", and 0.0349 for "News"). Additionally, the performance of model (20) was compared with that in

Liu et al. [16] using the "Football" CIF and QCIF sequence. Table 8 shows that the average RMSE of model (20) is smaller by approximately 0.5946 and 0.4550 compared with that in Liu et al. [16] for the "Football" CIF and QCIF sequences, respectively. Its average PCC is larger by approximately 0.0266 and 0.0173 compared with that in Liu et al. [16] for the "Football" CIF and QCIF sequences, respectively.

Table 5. Performance of model (21) and the model in [16] for "Foreman"

	Foreman.cif				Foreman.qcif			
	Model (21)		Liu et al. [16]		Model (21)		Liu et al. [16]	
SR	PCC1	RMSE1	PCC2	RMSE2	PCC1	RMSE1	PCC2	RMSE2
0.1	0.9937	0.1327	0.9673	0.2303	0.9956	0.1186	0.9660	0.2766
0.2	0.9956	0.1644	0.9673	0.3537	0.9967	0.1506	0.9660	0.3907
0.3	0.9985	0.1154	0.9673	0.5147	0.9985	0.121	0.9660	0.5711
0.4	0.999	0.1043	0.9673	0.6786	0.9993	0.0897	0.9660	0.7373
0.5	0.9994	0.0961	0.9673	0.6567	0.9996	0.0768	0.9660	0.956
0.6	0.9996	0.0876	0.9673	1.0956	0.9998	0.0645	0.9660	1.1424
0.7	0.9997	0.0802	0.9673	1.2567	0.9998	0.057	0.9660	1.2998
0.8	0.9998	0.0725	0.9673	1.3984	0.9999	0.0512	0.9660	1.4388
Average	0.9982	0.1066	0.9673	0.7731	0.9987	0.0912	0.9660	0.8516

Table 6. Performance of model (21) and the model in [16] for "News"

	News.cif				News.qcif			
	Model (21)		Liu et al. [16]		Model (21)		Liu et al. [16]	
SR	PCC1	RMSE1	PCC2	RMSE2	PCC1	RMSE1	PCC2	RMSE2
0.1	0.9976	0.0963	0.9648	0.3144	0.9976	0.0962	0.9645	0.3244
0.2	0.9986	0.0993	0.9648	0.4624	0.999	0.0828	0.9645	0.4672
0.3	0.9995	0.0719	0.9648	0.5854	0.9995	0.0666	0.9645	0.592
0.4	0.9997	0.0588	0.9648	0.6700	0.9997	0.0535	0.9645	0.6888
0.5	0.9998	0.0494	0.9648	0.7955	0.9998	0.0458	0.9645	0.8326
0.6	0.9999	0.0398	0.9648	0.8818	0.9999	0.0364	0.9645	0.9414
0.7	0.9999	0.0316	0.9648	0.9507	0.9999	0.0301	0.9645	1.0308
0.8	1	0.0254	0.9648	0.3144	1	0.0261	0.9645	1.1131
Average	0.9994	0.0591	0.9648	0.7086	0.9994	0.0547	0.9645	0.7488

Table 7. Parameters and performance of model (20) for "Football"

	Football.cif				Football.qcif			
	Model (21)		Liu et al. [16]		Model (21)		Liu et al. [16]	
SR	PCC1	RMSE1	PCC2	RMSE2	PCC1	RMSE1	PCC2	RMSE2
0.1	0.9771	0.2387	0.9697	0.3707	0.9703	0.2472	0.9726	0.3977
0.2	0.9874	0.2584	0.9697	0.4016	0.9798	0.3013	0.9726	0.3864
0.3	0.9915	0.2741	0.9697	0.5258	0.9885	0.2836	0.9726	0.4323
0.4	0.9958	0.2167	0.9697	0.6543	0.9928	0.2571	0.9726	0.5201
0.5	0.9976	0.1829	0.9697	0.8706	0.9953	0.2383	0.9726	0.7162
0.6	0.9986	0.1556	0.9697	1.0416	0.9968	0.2193	0.9726	0.897
0.7	0.999	0.1391	0.9697	1.1839	0.9977	0.2017	0.9726	1.0457
0.8	0.9993	0.1275	0.9697	1.301	0.9983	0.1845	0.9726	1.1775
Average	0.9933	0.1991	0.9697	0.7937	0.9899	0.2416	0.9726	0.6966

4 Joint Sampling-rate and Quantization Optimization

For 8-bit sequences, the number of bits can be derived by

$$R = f_R\left(SR, B\right) = SR \cdot N \cdot \left(8 - \log_2 QP\right) \qquad \textbf{(22)}$$

where N is the size of the block vector. Using $R = f_R\left(SR, B\right)$ and $D = f_D\left(SR, B\right)$, Figures. 11-13 show the RD curve for the "Forman", "Mother–daughter", and "News" sequences (CIF and QCIF formats) under the system shown in Figure 9 with fixed SR (from 0.1 to 0.8) as QP = 1, 2, 4, 8, 16, 32, 64, 128. For the same curve, different markers express different QP, and the eight markers from lower right to upper left correspond to QP = 1–256. Moreover, the solid line denotes the fitting curve based on the proposed RD model. From Figure 11, it can be seen that the practical

RD performance fits the proposed RD model (20) very well. Furthermore, Figures. 11-13 show that the distortion increases dramatically as QP increases from 16 to 128. Consequently, it is sensible to select $QP \in [1,16]$. Given fixed R_t, SR, and QP are the tradeoff of performance [24]. Additionally, for the same R_t, the minimum distortion is achieved without quantization if $SR \geq 0.1$ for the "Forman" and "Mother–daughter" sequences, which contain simple motion. This is primarily because the distortion caused by compressed sampling can be neglected when $SR \geq 0.1$ for simple motion sequences. Consequently, it is suggested that QP = 1 be selected when $SR \geq 0.1$ for simple motion sequences.

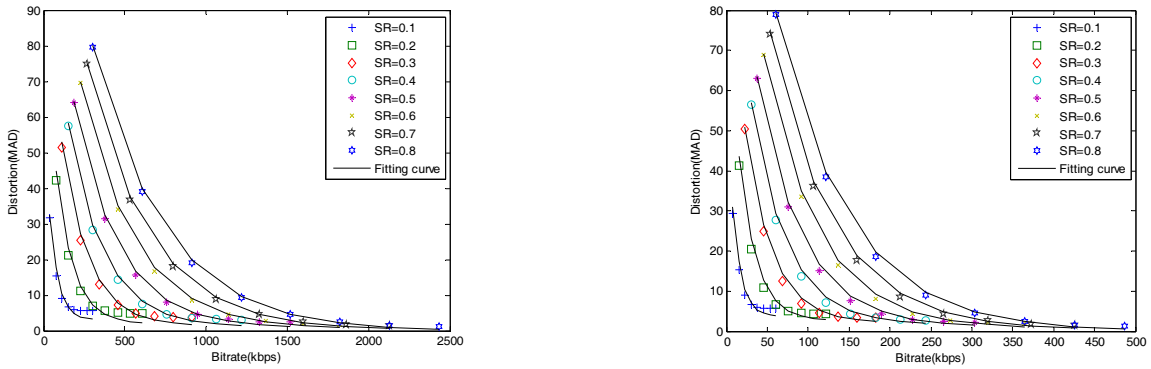

(a) Foreman.cif (b) Foreman.qcif

Figure 11. RD curve for "Foreman" sequences

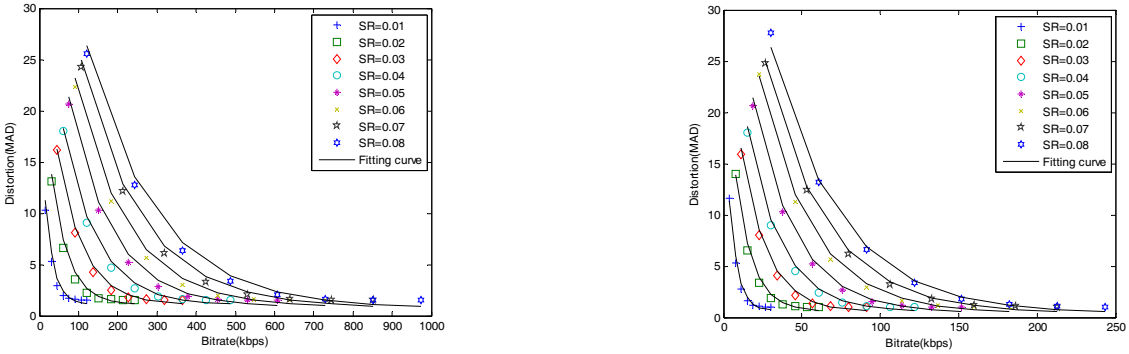

(a) Mother-daughter.cif (b) Mother-daughter.qcif

Figure 12. RD curve for "Mother–daughter" sequences

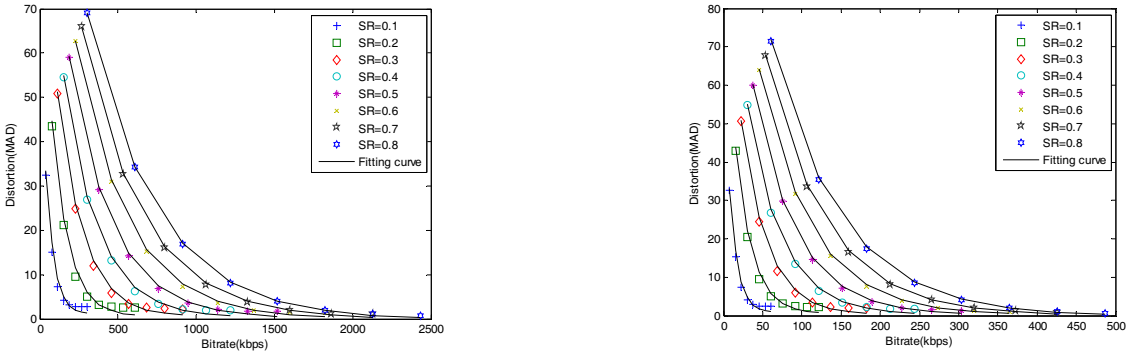

(a) News.cif (b) News.qcif

Figure 13. RD curve for "News" sequences

5 Simulation Results

Several numerical tests were conducted to evaluate the performance of the proposed algorithm within the framework shown in Figure 1. Several different video sequences, including "Mother–daughter", "Foreman", and "Football" (QCIF or CIF format), were tested in the simulations, and processing was carried out only on the luminance component. The size of GOP was set to 2, and the frame rate was fixed at 15 fps. The target bit-rate and the actual bit-rate by using the proposed rate allocation algorithm are shown in Table 8.

Table 8. Comparison between target measurement bit-rate and actual measurement bit-rate

QCIF				CIF			
Target bit-rate (Kbps)	Actual bit-rate (Kbps)			Target bit-rate (Kbps)	Actual bit-rate(Kbps)		
	Mother-daughter	Forman	Football		Mother-daughter	Forman	Football
300	300.3650	304.1280	285.1212	1000	998.2360	995.5247	973.2096
500	496.6048	486.6048	513.2256	2000	1995.6321	2003.2645	2007.2448
800	800.7328	790.7328	798.3467	3000	2979.3241	3001.5697	2919.6288
1000	1003.6224	1003.6224	1064.4576	4000	4011.3625	4023.6214	4044.4896
1200	1196.0992	1186.0992	1208.9146	5000	4956.3215	4968.3652	4896.4608
1500	1502.6400	1520.6400	1529.8179	6000	5981.2365	5985.6984	5960.9088

Finally, Figure 14 shows an example of the recovered 2nd frames in the "Football" QCIF sequence by using the conventional method with QP = 1 and SR = 0.6, and the rate allocation scheme with the target bit-rate set to 1800 kbps， which results in the average $QP=4$ and $SR=0.8$. Figure 15 shows the reconstructed 2nd frames in the "Forman" QCIF sequence by the conventional method with QP = 1 and SR = 0.2, and the rate allocation scheme with the target bit-rate set to 600 kbps， which results in the average $QP=4$ and $SR=0.8$. From Figures. 14 and 15, it can be seen that the subjective visual quality can be obviously improved by using the proposed rate allocation algorithm by approximately a 0.9~3.2 dB increase in PSNR (and smaller numbers of bits are required). That is, based on the above simulation results, it can be concluded that the proposed scheme has better RD performance by using the presented adaptive compressive sampling with rate allocation.

Figure 14. Recovered 2nd frame of "Football" (QCIF). (Left) Original frame. (Middle) Conventional scheme (QP = 1, SR = 0.6) 1835136 bits and 28.5991 dB. (Right) Proposed scheme (average QP = 4, SR = 0.8) 1824763 bits and 31.8660 dB.

Figure 15. Recovered 2nd frame of "Forman" (QCIF). (Left) Original frame. (Middle) Conventional scheme (QP = 1, SR = 0.2) 611712 bits and 34.3779 dB. (Right) Proposed scheme (average QP = 4, SR = 0.275) 607888 bits and 35.2008 dB.

6 Conclusion

5G wireless access solutions will consist of an evolution of LTE in combination with new radio access technologies. A rate control algorithm based on feedback channel was proposed to improve 5G wireless communication, so as for the RD performance of the DCVS system. A relatively accurate RD model was first established based on the assumption that the quantization distortion and the reconstruction distortion are independent, and then a training method was used to determine the parameters of the RD model at the decoder. Finally, the RD model as well as the target rate were applied to determine the optimal QP and SR, and then feed them back to the encoder as the parameters for the following frame. Experimental results demonstrated that the proposed method could improve the RD performance in the DCVS system without increasing the complexity of the encoder and time-delay.

Acknowledgements

This study was supported by research fund from Chosun University, 2017.

References

[1] R. F. Guiazon, K.-K. Wong, M. Fitch, Coverage Probability of Cellular Networks Using Interference Alignment under Imperfect CSI, *Digital Communications and Networks*, Vol. 2, No. 4, pp. 162-166, November, 2016.

[2] C. R. Panigrahi, J. L. Sarkar, B. Pati, Transmission in Mobile Cloudlet Systems with Intermittent Connectivity in Emergency Areas, *Digital Communications and Networks*, Vol. 4, No. 1, pp. 69-75, February, 2018.

[3] J. Dai, S. Wang, Clustering-based Interference Management in Densely Deployed Femtocell Networks, *Digital Communications and Networks*, Vol. 2, No. 4, pp. 175-183, November, 2016.

[4] X. Su, H. F. Yu, W. S. Kim, C. Choi, D. M. Choi, Interference Cancellation for Non-orthogonal Multiple access Used in Future Wireless Mobile Networks, *EURASIP Journal on Wireless Communications and Networking*, Vol. 2016, No. 1, pp. 1-12, December, 2016.

[5] X. Su, C. C. Liang, D. M. Choi, C. Choi, Power Allocation Scheme for Femto-to-macro Downlink Interference Reduction for Smart Devices in Ambient Intelligence, *Mobile Information Systems*, Vol. 2016, pp. 1-10, December, 2016.

[6] C. Choi, J. Choi, J. Shin, S.-R. Kim, P. Kim, Semantic Representation of Motion for Tracing Object in Surveillance System, *Journal of Internet Technology*, Vol. 13, No. 4, pp. 621-630, July, 2012.

[7] H.-J. Jeong, X.-F. Piao, J.-H. Choi, J.-Y. Shin, P.-K. Kim, Efficient Integration Method of Large-Scale Heterogeneous Security Logs Using NoSQL in Cloud Computing Environment, *Journal of Internet Technology*, Vol. 17, No. 2, pp. 267-275, March, 2016.

[8] D. Donoho, Compressed Sensing, *IEEE Transactions on Information Theory*, Vol. 52, No. 4 pp. 1289-1306, April, 2006.

[9] E. Candès, M. B. Wakin, An Introduction to Compressive Sampling, *IEEE Signal Processing Magazine*, Vol. 25, No. 2, pp. 21-30, March, 2008.

[10] M. Wakin, J. Laska, M. Duarte, D. Baron, S. Sarvotham, D. Takahar, K. Kelly, R. G. Baraniuk, Compressive Imaging for Video Representation and Coding, *Proceedings of Picture Coding Symposium (PCS)*, Beijing, China, 2006, pp. 711-716.

[11] J. Zheng, E. L. Jacobs, Video Compressive Sensing Using Spatial Domain Sparsity, *Optical Engineering*, Vol. 48, No. 8, pp. 1-10, August, 2009.

[12] T. T. Do, Y. Chen, D. T. Nguyen, N. Nguyen, L. Gan, T. D. Tran, Distributed Compressed Video Sensing, *Proceedings of the International Conference on Image Processing*, Cairo, Egypt, 2009, pp. 1393-1396.

[13] S. Ma, W. Gao, Y. Lu, Rate-distortion Analysis for H.264/AVC Video Coding and Its Application to Rate Control, *IEEE Transactions on Circuits and Systems for Video Technology*, Vol. 15, No. 12, pp. 1533-1544, December, 2005.

[14] M. Wu, X. Zhu, Z. Gan, X. Li, Adaptive Dictionary Learning for Distributed Compressive Video Sensing, *International Journal of Digital Content Technology and its Applications (JDCTA)*, Vol. 6, No. 4, pp. 141-149, March, 2012.

[15] Z. Liu, A. Y. Elezzabi, H. V. Zhao, Maximum Frame Rate Video Acquisition Using Adaptive Compressed Sensing, *IEEE Transactions on Circuits and Systems for Video Technology*, Vol. 21, No. 11, pp. 1704-1718, November, 2011.

[16] H. Liu, B. Song, F. Tian, H. Qin, Joint Sampling Rate and Bit-Depth Optimization in Compressive Video Sampling, *IEEE Transactions on Multimedia*, Vol. 16, No. 6, pp. 1549-1562, October, 2014.

[17] L. Gan, T. T. Do, T. D. Tran, Fast Compressive Imaging Using Scrambled Block Hadamard Ensemble, *Signal Processing Conference*, Lausanne, Switzerland, 2008, pp. 1-5.

[18] L. Wang, Y. Feng, Compressed Sensing of Hyperspectral Images Based on Scrambled Block Hadamard Ensemble, *Journal of Electronic Imaging*, Vol. 25, No. 6, pp. 1-9, December, 2016.

[19] Y. Pati, R. Rezaiifar, P. Krishnaprasad, Orthogonal Matching Pursuit: Recursive Function Approximation with Applications to Wavelet Decomposition, *Proceedings of Signals, Systems and Computers*, Pacific Grove, CA, USA, 1993, pp. 40-44.

[20] M. A. T. Figueiredo, R. D. Nowak, S. J. Wright, Gradient Projection for Sparse Reconstruction: Application to Compressed Sensing and Other Inverse Problems, *IEEE Journal of Selected Topics in Signal Processing*, Vol. 1, No. 4, pp. 586-597, December, 2007.

[21] L. Gan, Block Compressed Sensing of Natural Images,

Proceedings of the International Conference on Digital Signal Processing, Cardiff, UK, 2007, pp. 403-406.

[22] S. Mun, J. E. Fowler, Block Compressed Sensing of Images Using Directional Transforms, *Proceedings of the International Conference on Image Processing*, Cairo, Egypt, 2009, pp. 3021-3024.

[23] T. T. Do, Y. Chen, D. T. Nguyen, N. Nguyen, L. Gan, T. D. Tran, Distributed Compressed Video Sensing, *Proceedings of the International Conference on Image Processing*, Cairo, Egypt, 2009, pp. 1393-1396.

[24] E. W. Tramel, J. E. Fowler, Video Compressed Sensing with Multihypothesis, *Proceedings of the IEEE Data Compression Conference*, Snowbird, UT, 2011, pp. 193-202.

Biographies

Jinxiu Zhu received the Ph.D. degree in in Electric Power System and Automation from the Hohai University, Nanjing, China, in 2008. Currently, he is with the College of Internet of Things Engineering, Hohai University, China. His research interests include digital image/video processing and communications.

Christian Esposito received the Ph.D. degree in computer engineering and automation from the University of Napoli "Federico II", Naples, Italy, in 2009. He is currently an Assistant Professor with the University of Naples "Federico II". He serves as a Reviewer and the Guest Editor for several international journals and conferences (with about 200 reviews being done). He has been involved in the organization of about 40 international conferences workshops. His research interests include reliable and secure communications, middleware, distributed systems, positioning systems, multiobjective optimization, and game theory.

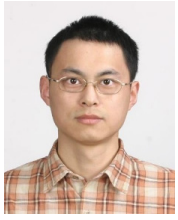

Aimin Jiang received the Ph.D. degree in electrical engineering from University of Windsor, Canada, in 2010. Currently, he is with the College of Internet of Things Engineering, Hohai University, China. His research interests include mathematical optimization and its applications to digital signal processing and communications.

Ning Cao received the B.S. and M.S. degrees in electrical engineering from Southeast University, Nanjing, China, in 1984 and 1990, respectively. He is now a professor with the College of Computer and Information, Hohai University, Nanjing, China. His current research interests include statistical signal processing, sensor array processing, and wireless communications.

Pankoo Kim received his B.E. degree from the Chosun University in 1988 and M.S. and Ph.D. degrees in Ccomputer Engineering from Seoul National University in 1990 and 1994. Currently, He is now working as a full professor at Chosun University. He is an editor-in-chief of IT CoNvergence PRActice (INPRA) Journal. His specific interests include semantic web techniques, semantic information processing and retrieval, multimedia processing, semantic web and system security.